Enhanced fan broadband noise prediction based on a 2D synthetic turbulence method

Carolin A. Kissner*, Attila Wohlbrandt†, and Sébastien Guérin‡
German Aerospace Center (DLR), Berlin, Germany

The prediction of fan broadband noise presents a challenge. Fully scale-resolving approaches are exceedingly demanding in computational resources, whereas analytical techniques rely on simplifying assumptions. RANS-informed synthetic turbulence methods are a compromise between accuracy and cost. In particular, a two-dimensional approach based on a simulation at midspan is attractive because it can easily be computed on a conventional PC. However, this approach raises some concerns: It is uncertain, if the mean flow and turbulence statistics at midspan are truly representative for the entire fan stage and if the neglect of three-dimensional flow effects is permissible. In this paper, the authors improve the current method to account for the three-dimensional nature of the flow by applying corrections based on turbulence spectra and by weighting results obtained at three spanwise positions at 20%, 50%, and 80% of the stator height. Cyclostationarity needs to be considered for all simulations as the resulting turbulence spectra cannot be described by conventional von Kármán spectra. Instead, the differing shape of the spectra can be attributed to turbulence in the wake and in the background flow. For this configuration, the deviation between the overall sound power at midspan and the overall sound power taking into account the three radial positions is less than 0.5 dB. Thus, the results at midspan are, in fact, representative for the entire fan as long as contributions close to the duct walls are ignored. Lastly, it is shown that non-linearities are negligible for the investigated, full-scale fan at approach.

I. Introduction

To maximize the efficiency of aircraft engines, state-of-the-art turbofans have larger-than-ever bypass ratios. The large bypass ratios of so-called Ultra-High Bypass-Ratio (UHBR) engines increases the relative contribution of tonal and broadband noise in a fan to the overall aircraft noise.

One key factor in achieving ambitious noise reduction goals is the fan noise, in particular the rotor-stator-interaction (RSI) noise. RSI noise is generated when rotor wakes impinge on the downstream leading edges (LEs) of the outlet guide vanes (OGVs). Its tonal component was thoroughly studied and technologies were developed to successfully reduce it. However, the understanding of broadband RSI noise is much less advanced. As the tones were significantly reduced, the relative contribution and therefore significance of the broadband noise due to the turbulence in the rotor wakes grew. Due to the stochastic nature of turbulence, the prediction of this noise generation mechanism presents a challenge. Used prediction approaches range from analytical to fully scale-resolving methods. In this paper, a hybrid method is used. A hybrid approach sequentially tackles each aspect of one physical problem with a separate, highly specialized method. Compared to analytical methods, it can account for complex geometries and flows. Compared to fully scale-resolving methods, less computational effort is required. Additionally, individual mechanisms involved in the broadband sound generation can be investigated separately. The chosen method combines a stochastic

*Research Engineer, Institute of Propulsion Technology, Department of Engine Acoustics, Müller-Breslau-Str. 8, 10623 Berlin, Germany, carolin.kissner@dlr.de.
†Research Engineer, Institute of Propulsion Technology, Department of Engine Acoustics, Müller-Breslau-Str. 8, 10623 Berlin, Germany.
‡Senior Research Scientist, Institute of Propulsion Technology, Department of Engine Acoustics, Müller-Breslau-Str. 8, 10623 Berlin, Germany.

method for synthesizing turbulence and a Computational AeroAcoustics (CAA) code for the generation and propagation of sound.

Recently, stochastic methods have been expanded to further investigate the impact of different aspects of turbulence on broadband RSI or airfoil-turbulence-interaction (ATI) noise. Strides in the development of three-dimensional modeling approaches as well as advances focusing on the synthesis of more realistic turbulence have been made.

A common method for synthesizing turbulence is the Stochastic Noise Generation and Radiation (SNGR) technique. The method that realizes target wavenumber spectra of turbulence via the superposition of Fourier modes was originally proposed by Kraichnan[1] and further developed by Bechara et al.,[2] Billson et al.[3] etc. Clair et al.[4] were the first to apply this method in three-dimensional space for studying ATI noise. The extension to three-dimensional space was successfully validated by comparing Amiet's analytical solution[5] to the far field solution determined via a (solid surface) Ffowcs-Williams-Hawkings (FWH) using the surface pressures on the blade. Gill et al.[6] also used this approach to study the impact of the contribution of the various gust components. They investigated one-component (transverse), two-component (transverse and streamwise) and three-component (transverse, streamwise, and spanwise) synthesized velocity fluctuations to realize Liepmann turbulence spectra and concluded that transverse velocity fluctuations are most relevant for symmetric airfoils at zero angle of attack. Following this argumentation, Polacsek et al.[7] also restricted the Fourier mode decomposition of the turbulence upstream of OGV's to the transverse velocity component. Non-linearized Euler equations were applied to propagate the synthesized turbulence. The authors investigated broadband RSI noise for a complete stator passage of the NASA SDT test case[8] as well as for a cascade consisting of four stator blades. Reboul et al.[9] took this work one step further and investigated sinusoidal leading edges using the same technique. They found differences in velocity spectra and root mean square surface pressures at different spanwise positions, which indicate that different spanwise positions have differing contributions to the overall sound power level. Another stochastic method that has been successfully applied to investigate three-dimensional ATI noise is the synthetic eddy method. It was originally proposed by Jarrin et al.[10] and further adapted for aeroacoustic simulations by Sescu and Hixon.[11] The method as applied by Kim and Haeri[12] injects turbulence into a CAA domain by randomly distributing eddies, which are described by an eddy shape function. The authors successfully applied the method for studying leading edge serrations and their numerical results conform to experimental data.

While the previously mentioned works have been restricted to the realization of homogeneous isotropic turbulence (HIT), some authors have attempted to investigate more complex forms of turbulence in their recent works. Gea-Aguilera et al.[13] used a method that prescribes Gaussian eddies directly in the CAA domain and expanded its formulation to realize spatially dependent turbulent length scales, thus realizing anisotropic, homogeneous turbulence.[14] Turbulent length scale ratios that are in agreement with measurements by Podboy et al.[15] for the NASA SDT test case were examined. Just recently, this method was expanded to three-dimensional space in order to study the influence of anisotropic turbulence on leading edge serrations.[16] Another recent development was introduced by Wohlbrandt et al.,[17] who demonstrated the consideration of cyclostationarity within a fan using a RANS-informed synthetic turbulence approach. URANS computations were used to provide fully periodic mean flow and turbulence characteristics as inputs for the fast Random Particle Mesh (fRPM) method and the CAA code. The fRPM was developed by Ewert[18] and synthesizes turbulent fluctuations by spatially filtering white noise. The fRPM method was expanded to realize cyclostationary turbulence, which was propagated within the periodic mean flow by the CAA code. The cyclostationary turbulence was prescribed in a vortex source domain, i.e. in a so-called fRPM patch. The prescribed turbulence was not homogeneous and had no directional preference. Nonetheless, a directional preference develops as the turbulence encounters the high mean flow gradients in rotor wakes. Thus, the realized turbulence was, in fact, inhomogeneous and anisotropic. In the paper, Wohlbrandt et al.[17] performed 2D simulations at 50% of the stator height for the NASA SDT fan to separately investigate the impact of the cyclostionarity of the turbulent kinetic energy (TKE), the turbulent length scale (TLS), and the mean flow on the broadband RSI noise. They concluded that a simulation using a constant mean flow and HIT can reproduce the results of a simulation using cyclostationary mean flow and turbulence if the prescribed, constant TLS is determined via a spectral averaging technique. However, they also postulated that this averaging technique only leads to identical results if either the wake or background turbulence is dominant.

Despite advances in the modeling and prediction of broadband fan noise, the fan broadband noise generation mechanism still needs to be better understood in order to specify the factors that have the greatest

impact on the noise levels. Only a detailed comprehension of fan broadband noise allows for the development of suitable noise abatement techniques.

In this paper, the authors expand the findings of Wohlbrandt et al.[17] and apply the fRPM method to a full-scale fan. In particular, the following questions are investigated:

- How representative is the midspan position chosen by Wohlbrandt et al.[17] for the prediction of RSI noise?
- How does the prediction change if the solutions of several, separately calculated simulations at different radial positions are averaged?
- How can the 2D approach be improved to yield a more accurate description of the noise generation mechanism e. g. by accounting for the difference in the wake turbulence statistics between the 2D and 3D CFD simulations?
- How relevant is the consideration of cyclostationarity?
- Do non-linearities influence the broadband RSI noise at approach conditions?

The first three research questions are the main focus of the paper, while the last two questions support the choice of methods used to answer the first questions. To improve the 2D approach, the authors apply the fRPM method at three different spanwise positions, i. e. at 20%, 50%, and 80% stator height. Periodic turbulence statistics and periodic flow are used. In addition, corrections are applied to account for three-dimensional flow effects as well as for the change in the wake between the turbulence seeding domain and the leading edge of the stator. The contribution of the three spanwise positions to the overall sound is analyzed. In a sense, this technique includes two distinct broadband noise generation mechanisms: RSI noise produced by the wake turbulence and ingestion noise caused by the background turbulence, which originates from the turbulence prescribed at the fan inlet. Usually methods that rely on the HIT approximation assume that the RSI noise is the dominant source and therefore neglect ingestion noise. Thus the turbulence length scale can be determined by multiplying the wake width by an empirical factor based on the work of Ganz et al.[19] This assumption is investigated by not only performing cyclostationary simulations but also simulations synthesizing HIT based on circumferentially averaged mean flow and turbulence statistics. The ingestion and RSI noise are studied separately to quantify their respective contribution to the overall fan broadband noise. Lastly, the used CAA code has only been used in combination with linearized Euler equations (LEE's) for fan applications in the past. However, other authors,[4,7,9] who use stochastic techniques to study ATI and/or RSI noise, standardly use non-linearized Euler equations. To analyze the influence of non-linearities on the fan broadband noise, the non-linearized Euler equations are applied for one simulation.

II. Method

A. Two-dimensional numerical methods

In the following section, an overview of the used technique is given. It will henceforth be denoted as fRPM-fan method and describes the application of the fRPM method to study fan broadband noise. The three methods comprised by the fRPM-fan method are discussed in more detail: the Computational Fluid Dynamics (CFD) method, the fast Random Particle Mesh (fRPM) method, and the Computational AeroAcoustics (CAA) method.

1. Overview of the fRPM-fan method

The fRPM-fan method consists of a number of separate methods and accommodates the realization of cyclostationarity in the mean flow and in the turbulence statistics of a fan stage.

Jurdic et al.[20] define a cyclostationary signal as a "random signal whose statistical characteristics vary periodically in time". Strictly speaking, two distinct types of cyclostationarity can be investigated using the fRPM-fan method: The mean flow exhibits cyclostationarity of order 1, i.e. that the signal itself exhibits a periodicity in time. Meanwhile, the turbulence exhibits cyclostationarity of order 2, since the turbulent velocity fluctuation is seemingly random but cyclostationarity can actually be found in its second-order statistics, i.e. in its turbulent kinetic energy and its turbulent length scale. While it is technically possible

to investigate these types of cyclostationarities separately,[17] it was not done in this paper. For simplicity's sake, the authors do therefore not distinguish between these two types of cyclostationarity. Simulations that consider cyclostationarity in its mean flow and turbulence statistics are described as "cyclostationary" or "periodic". Simulations that do not consider cyclostationarity and instead rely on circumferentially averaged values are referred to as "steady". Examples for both types of simulations are shown in Figure 1.

The fRPM-fan method is a hybrid method consisting of multiple, highly specialized approaches. A URANS simulation provides the mean flow and turbulence statistics that are used as inputs by the fast Random Particle Mesh (fRPM) method and the Computational AeroAcoustics (CAA) code. The fRPM method reconstructs turbulence based on the turbulent kinetic energy (TKE), the turbulent length scale (TLS), and a suitable assumption regarding the correlation function. The synthesized turbulence is coupled into the CAA domain and propagated within the mean flow. The turbulence interacts with the stator leading edge generating broadband noise. The CAA propagates the sound to the sensor positions at which the sound power can be determined.

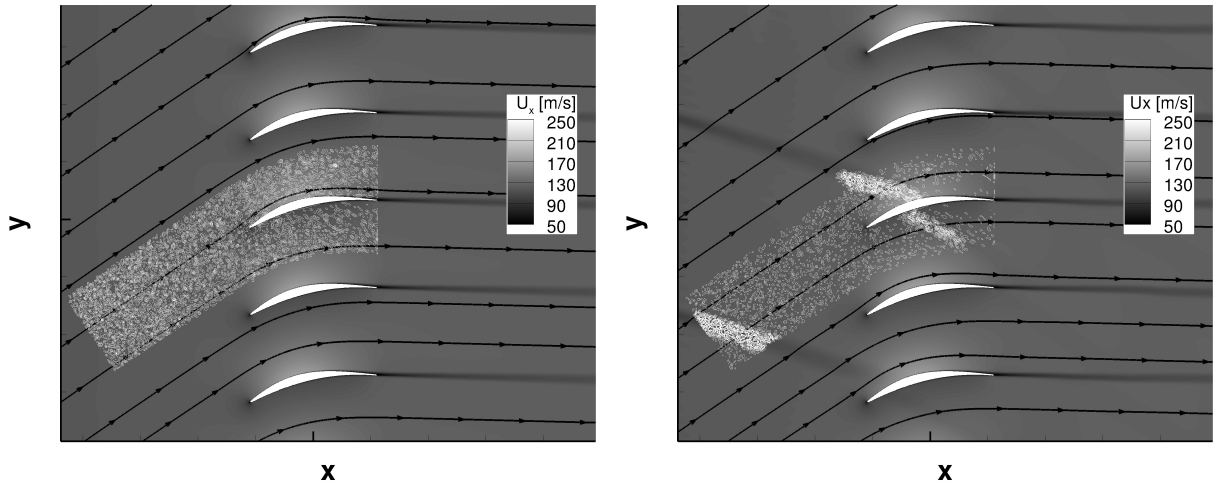

(a) Steady (b) Periodic

Figure 1. Comparison of simulations: constant and periodic turbulence statistics and mean flow. Vorticity and axial flow velocity shown.

2. Computational Fluid Dynamics (CFD) - mean flow and turbulence statistics

The DLR in-house solver TRACE[21] was used to perform all CFD simulations. The SSG/LRR-omega full Reynolds Stress turbulence model[22] was used as it accurately determines turbulent statistics in relevant regions near the stator leading edge and in the wake. A MUSCL (Monotonic Upstream Scheme for Conservation Laws) method of second order accuracy based on Fromm's scheme was applied for the spatial discretization and an Euler Backward scheme of second order accuracy, for the time discretization. The turbulence at the inlet boundary of the fan stage was defined by a turbulence intensity of 1% and integral turbulent length scale of 0.01 m.

3. Fast Random Particle Mesh (fRPM) method - turbulence synthesis

The Random Particle Mesh (RPM) method, introduced by Ewert,[18] synthesizes time-space-dependent turbulent fluctuations using the background flow, the turbulent kinetic energy k_t, and the integral turbulent length scale Λ provided by the CFD simulations.

In this paper, the method was applied as follows: White noise is spatially filtered by a superposition of Gaussian filters of given length scales in order to realize a von Kármán spectrum, whose length scale corresponds to the TLS extracted from the URANS simulation. The superposition of Gaussian spectra of various length scales using analytical weighting functions was introduced by Wohlbrandt et al.[23] The filtered turbulent field is then scaled with the variance, which corresponds to the turbulent kinetic energy, and convected with the background flow speed $\mathbf{u}_0$.

The derivation of the RPM method is not restricted to a spatially constant variance, length scale, or mean flow. This fact was used in realizing cyclostationarity. The method uses the local variance, length scale, and background flow at each elemental volume at the inlet of the vortex source and realizes a von Kármán spectrum fulfilling these desired local turbulence characteristics. As the local turbulence and mean flow changes periodically in time when realizing cyclostationarity, the realized turbulence is inhomogeneous even though von Kármán spectra are realized. The turbulence develops a directional preference as it is convected in a mean flow with strong mean flow gradients due to the wake structure. Hence, an inhomogeneous, anisotropic turbulence is realized by the fRPM method when considering cyclostationarity.

In this paper, the authors worked with the fast Random Particle method,[24] which uses recursive filters on a Cartesian grid to speed up the computation.

4. Computational AeroAcoustics (CAA) - convection of synthesized turbulence, generation and propagation of acoustic waves

The acoustic and turbulent fluctuations are solved in the time domain by the CAA solver PIANO.[25] For this work, the low-dispersion low-dissipation Runge-Kutta method[26] was used for the time integration and the dispersion-relation-preserving finite difference scheme by Tam and Webb,[27] for the spatial discretization. The code was applied to solve the linearized as well as the non-linearized Euler equations. The non-linearized Euler equations or PErturbed Nonconservative Nonlinear Euler Equations (PENNE) were introduced by Long[28] and can be derived from the Navier-Stokes equations in perturbation form.[29] Taking advantage of the periodicity in a fan, all flow variables $\phi_0(t)$ can be set to

$$\phi_0(t) = \sum_{k=0}^{\infty} \phi_k^0 e^{-ik\omega t}, \tag{1}$$

where ϕ_k^0 is the k^{th} harmonic of the base frequency ω and $k = 0$ represents the steady part $\phi_0^0 = \overline{\phi_0(t)}$. Thus, cyclostationarity can be realized by adding up the complex Fourier coefficients at each time step.

The turbulence synthesized by the fRPM method is coupled solenoidally into the CAA domain by the LEE-relaxation formulation.[29] A relaxation term is added to the impulse equations,

$$\frac{\partial u_i'}{\partial t} + \cdots = -\epsilon_{ijk} \frac{\partial}{\partial x_j} \left[\sigma \left(\Omega_k' - \Omega_k^{\text{ref}} \right) \right], \tag{2}$$

where σ is the forcing parameter, Ω_k' is the vorticity given by the left hand side of this equation as

$$\Omega_k' = \epsilon_{ijk} \frac{\partial u_k'}{\partial x_j}, \tag{3}$$

and Ω_k^{ref} is the externally imposed fluctuating reference vorticity. For best results, the forcing parameter σ should be chosen to be as large as stability limits permit.

B. Additional pre- and post-processing operations

Post-processing techniques, that will be applied to the results in Section IV, are introduced in this section. Sound power level and velocity frequency spectra characterizing von Kármán turbulence are discussed. In addition, two different averaging techniques are shown for determining the TLS at a particular spanwise position.

1. Sound power level

The analyses in Section IV are based on sound power level spectra, total sound power levels, and upwash velocity frequency spectra. The power spectra are determined assuming that the respective 2D computation is representative of a corresponding radial section of the duct. The intensity at each sensor position (i) is thus multiplied by an equivalent area segment spanning a respective duct height ΔA_i. The sound powers of all sensors N are then summed up and multiplied by a correction factor, that corrects 2D to 3D turbulence as the CAA simulations were restricted to two-dimensional space:

$$P = Q_{2D \to 3D} \sum_{i}^{N_\vartheta} I_i \Delta A_i \tag{4}$$

with

$$Q_{2D\to 3D} = \frac{S_{22}(k_1)}{S_{22}^{2D}(k_1)} = \frac{1}{10}\left(3\hat{k}_1^{-2} + 8\right), \tag{5}$$

where N_ϑ signifies the number of sensors (see Figure 2). The sound power level can be computed as

$$L_W = 10\log_{10}\left(P/\,P_{\mathrm{ref}}\right), \tag{6}$$

where the reference sound power P_{ref} equals 1×10^{-12} W.

2. Velocity spectra

In this investigation, the RPM method realizes von Kármán turbulence spectra. For the purpose of validating numerical velocity frequency spectra based on a one-dimensional wavenumber, the analytical spectra in flow direction and perpendicular to the flow are given as:

$$S_{11}(k_1) = \frac{2u_t^2\Lambda}{\pi}\frac{1}{(1+\hat{k}_1^2)^{5/6}}\frac{2\pi}{u_0} \tag{7}$$

$$S_{22}(k_1) = \frac{2u_t^2\Lambda}{2\pi}\frac{1+\frac{8}{3}\hat{k}_1^2}{(1+\hat{k}_1^2)^{11/6}}\frac{2\pi}{u_0} \tag{8}$$

with the convective wavenumber $k_1 = \omega/u_0$, the integral length scale (TLS) Λ, the turbulence velocity variance u_t and the reduced wavenumber $\hat{k} = k/k_e$ with $k_e = \frac{\sqrt{\pi}\Gamma(5/6)}{\Lambda\Gamma(1/3)}$. The upwash velocity frequency spectrum differs for 2D turbulence:

$$S_{22}^{2D}(k_1) = \frac{10u_t^2\Lambda}{3\pi}\frac{\hat{k}_1^2}{\left(1+\hat{k}_1^2\right)^{11/6}}\frac{2\pi}{u_0} \tag{9}$$

In this work, the authors restrict all analyses to the 2D upwash velocity frequency spectra (see Eq. 11) as this component is more important for the noise generation mechanism at the stator leading edge. Investigating spectra in both directions would not enhance the findings as the information is redundant.

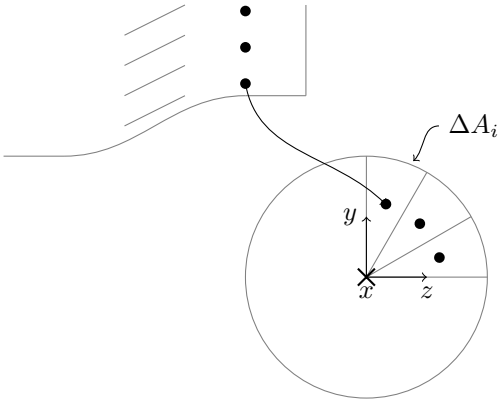

Figure 2. Sketch of sensors in 2D CAA domain and their equivalent positions in a 3D duct for the determination of sound power levels. Sensor positions (i) indicated by black dots and duct area segments denoted by ΔA_i.

3. Determination of the turbulent length scale (TLS) for a simulation without cyclostationarity

A turbulent length scale (TLS) can be determined in multiple ways. Two averaging techniques, that are applied in this paper, are shown here.

Circumferential averaging A circumferential averaging is used automatically when performing a steady simulation. To determine the TLS, circumferential averages of the TKE k_t, the turbulent dissipation rate ω_t, and the mean flow velocity u_0 need to be extracted from the q3D simulations to describe the mean flow and the turbulence statistics. The circumferential averages are determined by

$$k_t^C = \frac{1}{2\pi}\int_0^{2\pi} k_t(\vartheta)d\vartheta, \qquad \omega_t^C = \frac{1}{2\pi}\int_0^{2\pi} \omega_t(\vartheta)d\vartheta, \qquad u_0^C = \frac{1}{2\pi}\int_0^{2\pi} u_0(\vartheta)d\vartheta. \tag{10}$$

From these values, an integral turbulent length scale could be directly determined:[30]

$$\Lambda = \frac{C_{\mathrm{Re}}}{C_\mu}\frac{\sqrt{k_t^C}}{\omega_t^C}, \tag{11}$$

where the $C_\mu = 0.09$ represents a constant, which is dependent on the formulation of the turbulence model, and C_{Re} depends on the Reynolds number as described by Donzis et al.[31] For high Reynolds numbers, C_{Re} asymptotically approaches a value of 0.4. Therefore, C_{Re} was set to 0.4 in this work.

SPECTRAL AVERAGING The second averaging technique is inspired by the periodic simulations. When cyclostationarity is considered, the fRPM method applies the prescribed correlation function at each point at the inflow of the fRPM patch using the local mean flow and turbulence characteristics. Thus, a circumferentially averaged velocity frequency spectrum based on local spectra can be calculated at any axial position:

$$S_{ii}^{\mathrm{P}}(f) = \frac{1}{2\pi} \int_0^{2\pi} S_{ii}(f, \vartheta) d\vartheta. \tag{12}$$

If needed a TLS value can be determined by fitting this circumferentially averaged velocity frequency spectrum (see Eq. 14) with an equivalent von Kármán spectrum. This method works well if either the wake or the background turbulence is dominant.

III. Application

The fRPM-fan method was applied to the ASPIRE fan configuration. The fan geometry is generic, yet realistic for a modern fan stage of an UHBR engine. The target bypass ratio is 16 and the in-flight minimum engine thrust was chosen to be comparable to a typical engine of a modern, mid-sized passenger aircraft with two underwing engines. The fan stage has a cut-off design with 16 rotor blades and 36 OGV's. Details regarding the operating conditions at approach are given in Table 1.

In this section, the test matrix and the setups of the individual methods needed for the study of fan broadband noise, namely CFD, CAA, and fRPM, are discussed.

Table 1. Fan characteristics and approach operating point of investigated configuration

Target bypass ratio	16
Number of rotor blades	16
Number of stator blades	36
Relative rotational speed N_1	56%
Fan pressure ratio	1.096
Axial Mach number	0.23
Rotor Tip Mach number	0.56

A. Definition of test matrix

Eight different simulations were performed. An overview of these simulations is given in Table 2. The identifiers introduced in Table 2 are used to denote the simulations during the course of this work. The first three simulations investigate the fan broadband noise at three different spanwise positions. Cyclostationarity was considered and LEE's were applied. The last five simulations were done to validate the chosen approach of the first three simulations by investigating the influence of cyclostationarity and non-linearities.

Table 2. Test matrix of simulated configuration

identifier	description	cyclostationary?	non-linearities?
P-20	at 20% stator height	yes	no
P-50	at 50% stator height	yes	no
P-80	at 80% stator height	yes	no
C-50	constant turbulence and mean flow	no	no
C-50-tls	alternative TLS (spectral average)	no	no
C-50-wake	wake TLS and TKE	no	no
C-50-background	background TLS and TKE	no	no
P-50-PENNE	including non-linear terms	yes	yes

The spanwise positions are shown on a slice in the rotor domain (see Fig. 3). The axial position of the slice was chosen to be located in the rotating domain of the 3D RANS computation slightly downstream of the rotor trailing edge. The TKE and TLS are shown. The spanwise positions were chosen to be representative of the entire duct, while avoiding the wall boundary layers and areas of flow separation near the hub and tip walls of the duct. The chosen spanwise positions were located at 20%, 50%, and 80% of the stator height.

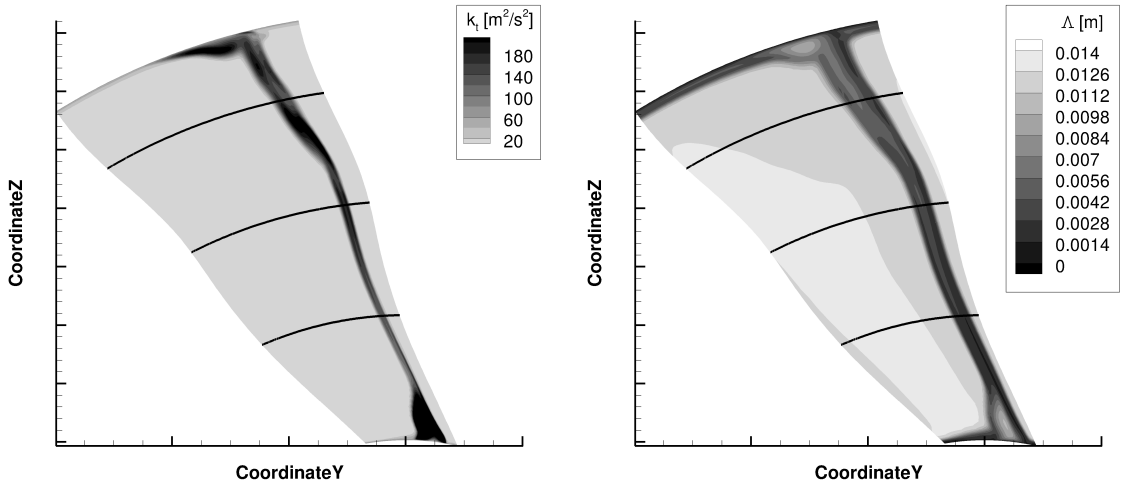

(a) TKE (b) TLS

Figure 3. Slice showing the rotor wake in rotating domain. Contours of the turbulent kinetic energy k_t and of the integral turbulent length scale Λ are shown. Lines indicate the streamtraces corresponding to 20%, 50%, and 80% of the stator height.

Cases C-50 and C-50-tls were performed to show the effect of the cyclostationarity in the turbulence and mean flow. The C-50 simulation used a circumferentially averaged background flow as well as circumferentially averaged turbulence statistics. In contrast, the C-50-tls used a spectrally averaged TLS value.

The computation time for the reference case P-50 amounted to 4.5 days on 11 Intel(R) Xeon(R) CPU's E7-4830 v3 @ 2.10GHz. The computation time depends on the grid size, the largest permissible time step, and the total amount of time steps. The largest allowed time step depends on the smallest cell in the grid and total amount of time steps was chosen so that all simulations consider 50 rotor wakes. If a constant simulation instead of a periodic simulation is performed, the total computation time decreases by about half. Using non-linearized Euler equations instead of LEE's increases the computation time by nearly 20%.

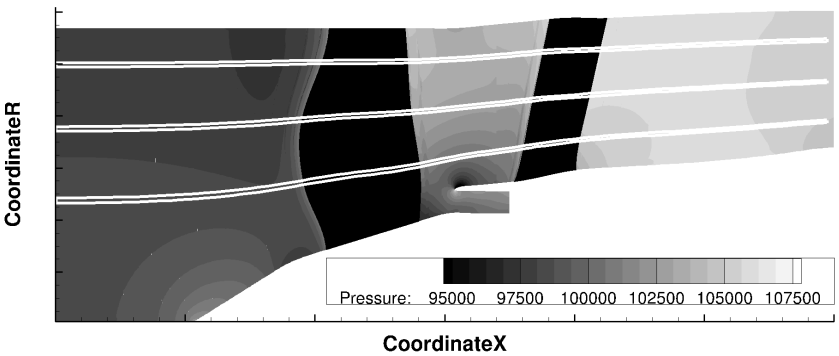

Figure 4. Q3d URANS domains shown in the fan stage. The contour shows the pressure distribution of the 3D RANS computation.

B. CFD setup

For this paper, a 3D RANS and three q3D URANS simulations were required. The 3D RANS simulation is needed to extract streamlines at the chosen spanwise to set up the q3D URANS simulations (see Fig. 4). Periodic boundary conditions were applied to the q3D URANS simulations. Thus, the URANS simulations contained four rotor and nine stator blades. In the stator domain, unsteady solutions of the first 15 harmonics were needed to correctly reproduce the wake structure in the absolute domain of reference. The number

of required harmonics mainly depends on the flow gradients; more harmonics are needed to resolve steeper gradients. It should be noted that using fewer harmonics still yields reasonable sound power level spectra but the wake structures are corrupted by large harmonic undulations. While the influence of these corrupt wake structures are not visible when using a stationary spectral analysis, they would be using a cyclostationary spectral analysis. In the stator domain, the mean flow, i.e. the 0th harmonic, is obtained via a flux averaging between the moving frame of reference of the rotor block and the absolute frame of reference in the stator block. For cases C-50 and C-50-tls, only the 0th harmonic was considered.

The investigated operating point was approach and parameters were provided for the 3D RANS (see Table 1). The q3D domains are essentially 2D flows. The rotor wake is only dependent on the incidence angle of the rotor blade for 2D flows. Hence, the operating point of the q3D URANS simulations were set to match the incidence angle of the 3D RANS at the equivalent streamline position. The incidence angles of the rotor are shown in Fig. 5. The offset in incidence angles between URANS simulations and the 3D RANS computation was small. Of course, 3D effects were thus neglected in the q3D simulations. A correction that considers 3D flow effects was introduced in Section 2.

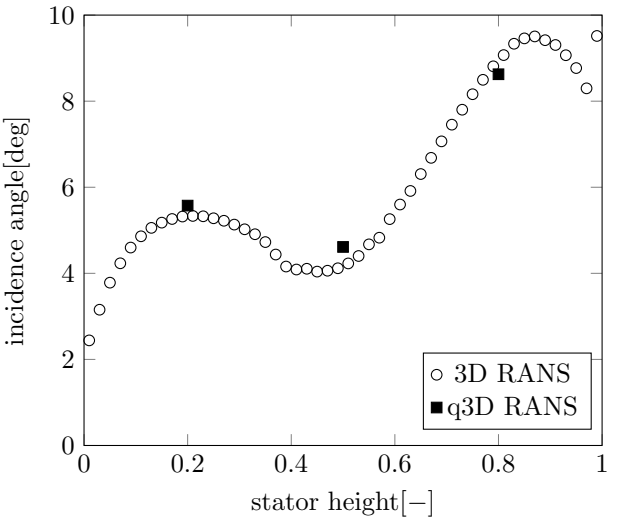

Figure 5. Incidence angles of the rotor shown for 3D RANS and q3D URANS computations at equivalent streamline positions.

C. CAA/fRPM setup

Figure 6 displays the CAA setup for predicting the fan broadband noise of the ASPIRE fan with the fRPM method. The setup at 50% of the stator height contains the positions of vortex source, vortex sink, sponge zones, and sensors relative to the stator vanes.

The vortex source is an fRPM patch that injects synthetic turbulence into the CAA domain about two chord lengths upstream of the stator leading edge. The fRPM patch was rotated into the direction of the flow so that no buffer zone accounting for the lateral convection was necessary. The region of the patch that actively produces turbulence spans exactly one pitch; the rest of the patch area contains safety margins. It is assumed that the vanes are acoustically uncorrelated and that it is therefore permissible to excite only one blade. This assumption has been proven to be correct in.[17] The remaining blades only ensure the correct acoustic radiation due to cascade effects (the solidity of vanes was greater than one[32]). The CAA domain contains nine instead of 36 vane blades. Periodic boundary conditions are still valid and no differences to a simulation considering the full duct are expected, as all circumferential modes are already cut-on in a duct containing the reduced amount of stator blades within the investigated frequency range. The cell size as well as the mean flow of the vortex source and CAA domains match.

The vortex sink uses the LEE-relaxation method to remove vortices downstream of the stator trailing edges. The vortices tend to interact with the stator wake resulting in hydrodynamic pressure fluctuations. As only the acoustic pressure fluctuations are of interest, the vortices are removed by setting the target vorticity to zero.

Sponge zones were placed at the in- and outlet boundaries to avoid acoustic reflections. An additional cell stretching - not exceeding a value of 1.1 - was applied.

The sensors were equally spaced up- and downstream of the stator. At these positions, sound power levels were computed under the assumption that the 2D simulation at a given stator height is representative for the entire duct and that the blades are acoustically uncorrelated.

D. CAA/fRPM mesh generation

High-order spatial discretization schemes require a high grid quality in the computational domain. The chosen grid resolution depends on two factors: acoustics and turbulence.

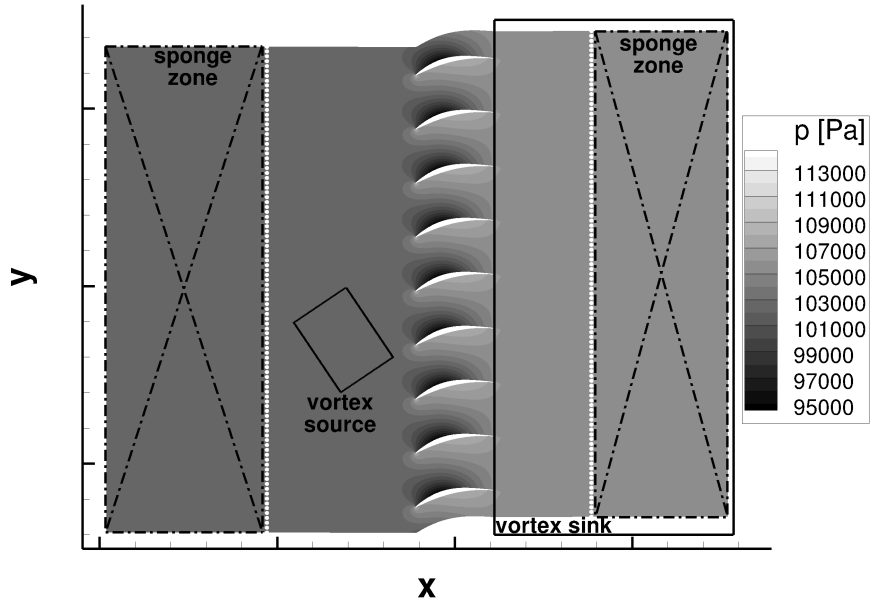

Figure 6. CAA setup with nine stator vanes at 50% stator height. Sponge zones, vortex source, and vortex sink are shown. White dots indicate sensor positions and the countour plot shows the pressure of the mean flow.

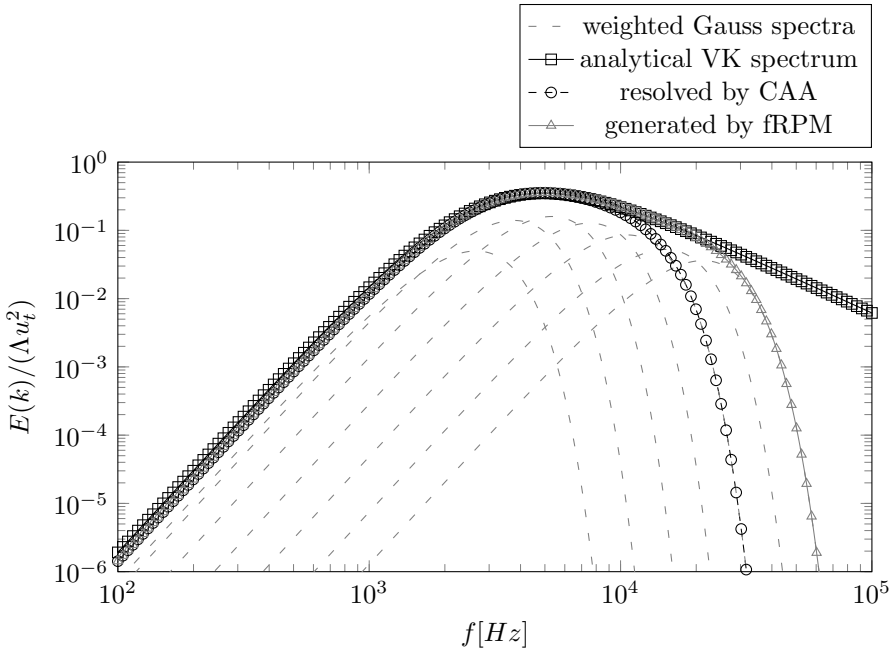

Figure 7. Realization of turbulent energy spectra for the smallest integral turbulent length scale in the rotor wake at 50% of the stator height.

The CAA mesh was designed to propagate sound waves up to a frequency of 10 kHz without significant dissipation. The minimal acoustic resolution was chosen to be 7 points per wavelength (PPW), which complies with the theoretical resolution limit of 5.4 PPW for a Dispersion-Relation-Preserving (DRP) scheme.[33] This leads to a grid size of $dx_f = \frac{\lambda}{\mathrm{PPW}} = 0.00486$ m.

The grid size has to be smaller in regions of the grid, where turbulence is injected into and convected in the domain. The same grid sizes were used in the fRPM and CAA domain. To determine the cell size needed for resolving turbulence in the CAA up to a frequency of 10 kHz, a theoretical analysis was performed for the smallest and thus critical length scale in the wake near the stator leading edge. The von Kármán spectrum is realized by the superposition of seven Gaussian turbulence spectra in the fRPM domain. The aim of the analysis was to determine the smallest Gaussian TLS, which dictates the required cell size. The CAA domain is more critical in terms of the turbulence resolution, since it requires four cells to fully resolve a vortex structure instead of two in the fRPM domain. Particularly at higher frequencies, the turbulent energy therefore drops more quickly in the CAA than in the fRPM domain as can be seen in Figure 7. The minimum Gaussian TLS is adjusted until the CAA resolution suffices for resolving the turbulence up to a frequency of 10 kHz. The cell size is equal to twice the determined minimum Gaussian TLS. Resulting turbulent resolutions dx_v are shown in Table 3.

Lastly, a no-slip boundary condition was applied at the stator surfaces, even though the boundary layer was not fully resolved by the meshes. Neglecting the boundary layer entirely can lead to the generation of artificial sound at a blunt trailing edge (TE). As vortices move along the surface, they create sound when interacting with the blunt TE. The boundary layer prevents the direct interaction between the TE and the vortices as the vortices are pushed further away from the surface, which reduces the trailing edge noise radiation.

Table 3. Mesh sizes of CAA grids at different spanwise positions

stator height [%]	dx_v [m]	mesh size [cells per passage]
20	0.001125	103,824
50	0.001250	110,024
80	0.001000	174,092

IV. Results and discussion

In the following section, the results of the test matrix are discussed. At first, the simulations at different spanwise positions were analyzed. The simulations were performed using linearized Euler equations and considering the cyclostationarity in the mean flow and the turbulence statistics. The contribution to the overall power levels of each of those simulations were quantified. In a next step, the validity of the chosen approach of the previous simulations (P-20, P-50, and P-80) are to be undermined by investigating the effects of cyclostationarity and of non-linearities.

A. Fan broadband noise at different spanwise positions

To quantify the fan broadband noise at the respective spanwise positions and to determine their contributions to the overall sound power levels, interim steps were necessary. At first, it was checked that the fRPM method correctly realizes the prescribed, cyclostationary turbulence. In a next step, corrections were applied to account for three-dimensional flow effects that were naturally absent in the q3D computations and to account for the wake development between the patch position and the stator leading edge.

1. Analysis of analytical and numerical velocity frequency spectra

Averaged, analytical transverse velocity frequency spectra as well as the local spectra at circumferential positions within one rotor passage are shown in Fig. 8. For the different duct heights in the corresponding subfigures, the contribution of background and wake turbulence to the overall turbulence can also be seen. Spectra with lower peaks at lower frequencies can be directly attributed to the background turbulence, while spectra with higher peaks at higher frequencies can be attributed to the wake turbulence. For this configuration without any applied corrections, it can be said that the background turbulence dominates at lower frequencies and the contribution of the wake turbulence starts at a frequency of 1 kHz. For the

uncorrected spectra, the influence of the wake turbulence is largest at a stator height of 20% and smallest at a stator height of 80%.

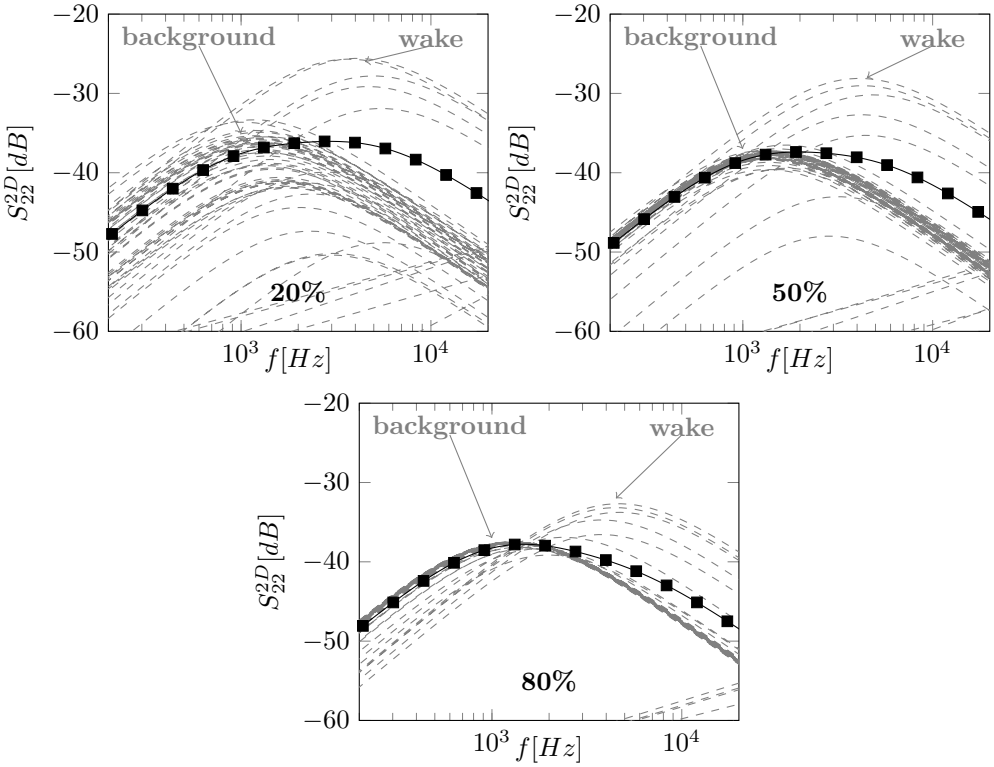

Figure 8. Averaged transverse velocity frequency spectra shown by black, solid lines. Gray, dashed lines show local transverse velocity frequency spectra calculated at circumferential positions within one rotor passage.

A sensor was positioned in the vortex source and transverse velocity frequency spectra were determined. A comparison with the analytical spectra shows that the fRPM method is able to reproduce these spectra (see Fig. 9). This indirectly proves that the fRPM method is capable of synthesizing the prescribed, cyclostationary turbulence. The figure also shows that the intended resolution of turbulence up to a frequency of 10 kHz was achieved by all simulations.

2. Corrections for 3D flow effects and wake development

The two-dimensional CAA simulations at different spanwise positions neglect two effects: (1.) Changes in the wake: The turbulence is directly prescribed at the position of the patch and this prescribed, frozen turbulence interacts with the stator leading edge to produce noise. In reality, the turbulence decays and the wake structure changes as the wake gets more diluted with an increasing distance from the rotor. (2.) 3D flow effects: The q3D URANS simulations cannot consider 3D flow effects. For instance, wake structures can be influenced by spanwise velocities induced by areas of flow separation. Since spanwise velocities cannot exist in a q3D simulation, such phenomena cannot be reproduced.

Correction curves give corrections as a function of the frequency and are used to correct for the changes in the wake as well as for 3D flow effects. An analogous approach was used for both corrections. Since the authors assume that the streamwise velocity fluctuations are mainly responsible for the noise generation at the stator leading edge, correction curves were computed based on the difference in the analytical upwash velocity frequency spectra (see Eq. 11). The corrections are added to the sound power level spectra in Section 2. The correction curve to account for changes in the wakes was determined by taking the difference in the upwash velocity frequency spectra at the stator leading edge and at the patch position in the respective q3D domain (see positions 2 and 3 in Fig. 11). To account for 3D flow effects, the correction curve was determined at a position in the rotor domain (see position 1 in Fig. 11). The velocity spectrum of the q3D simulation was deducted from the spectrum of the URANS computation. The upwash velocity frequency

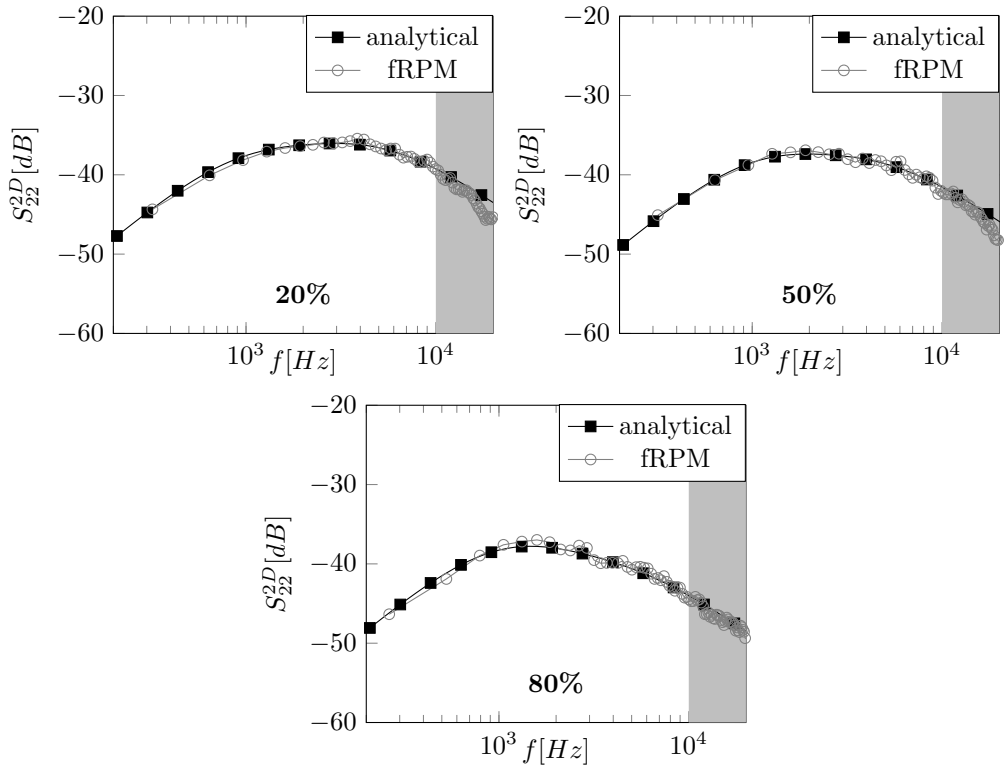

Figure 9. Upwash velocity frequency spectra realized by the fRPM method compared to respective analytical spectra. The gray boxes indicate the limit of the mesh resolution.

spectra used in determining the correction curves at the different positions are depicted in the Appendix in Fig. 19 and Fig. 20.

Figure 10 shows the correction curves that were used to correct for changes in the wake and for 3D flow effects at each spanwise position. The changes due to the developing wake between the patch position and the stator leading edge lead to a negative correction value and therefore a decrease in the power spectra. This is quite plausible as the TKE decreases with an increasing distance from the rotor and TKE is directly related to the amplitude of the velocity frequency spectra. The correction value decreases with an increasing frequency. The correction curves used to account for 3D flow effects differ noticeably for the three simulations. While the corrections of the 3D flow effects at 20% and 50% of the stator height are moderate, the correction at 80% of the stator height is relatively large. However, that result is reasonable when considering the flow behind the rotor in the 3D RANS computation (see Fig. 3). There is a large area of flow separation near the tip wall. Areas of flow separation cause spanwise flows and tend to increase the wake turbulence in neighboring areas. Thus, the turbulence in the wake increases significantly at 80% of the stator height.

The initial power spectra up- and downstream of the fan are shown in Fig. 12. No corrections have been applied yet and the grey areas in the graphs indicate the limit of the mesh resolution. In that area, some dissipation effects can be expected. Figure 13 shows the corrected power spectra. The influence of each correction on the sound power spectra at the respective spanwise positions can be seen in Appendix in Fig. 21, Fig. 22, and Fig. 23. When looking at the overall sound power level before and after applying the corrections in Table 4, then the change at 80% of the stator height was most significant amounting to an increase of about 7 dB. At 50% of the stator height, the corrections yielded a 2 dB increase in the overall sound power level. Lastly, there was a decrease of about 2 dB at 20% of the stator height.

3. Sound power levels of the entire duct

All spectra have been computed under the assumption that the broadband noise at the respective spanwise position is representative for the entire duct. Figure 13 indicates that the fan broadband noise increases with increasing radial height for this configuration at the investigated operating point.

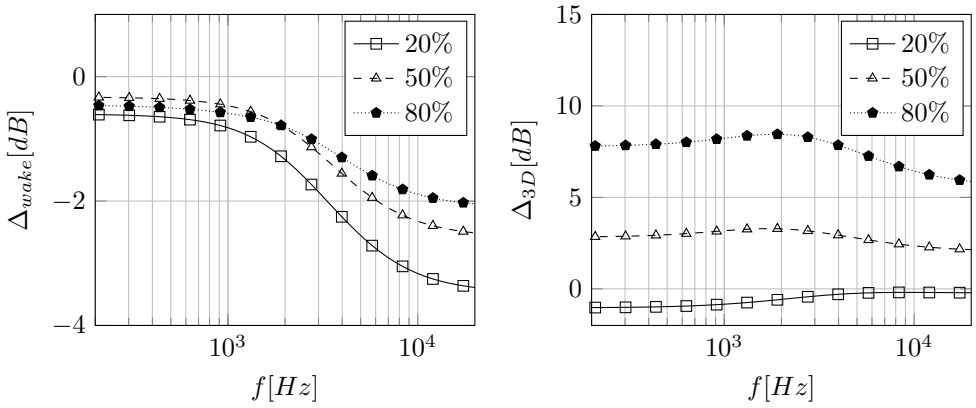

(a) wake changes (b) 3D flow effects

Figure 10. Correction curves of all spanwise positions.

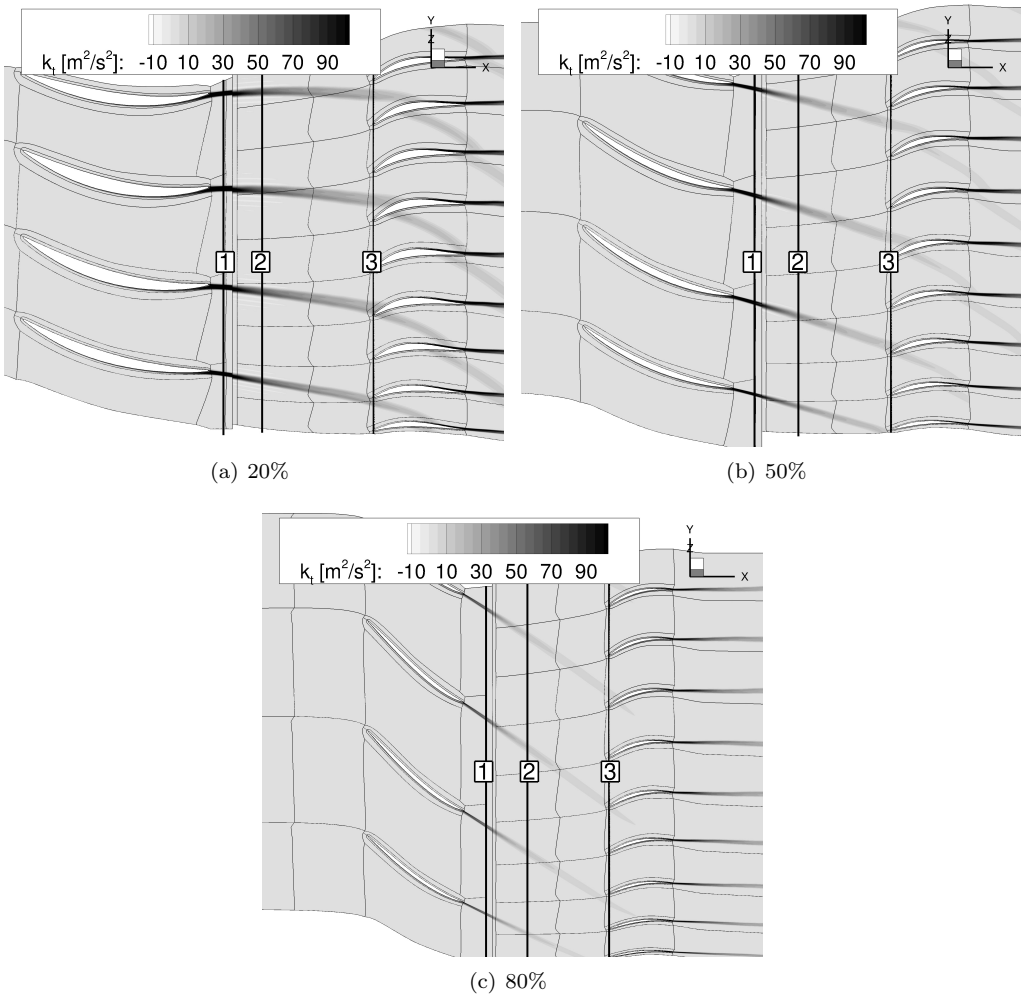

(a) 20% (b) 50%

(c) 80%

Figure 11. Contour of TKE and positions which were used to calculate correction curves shown.

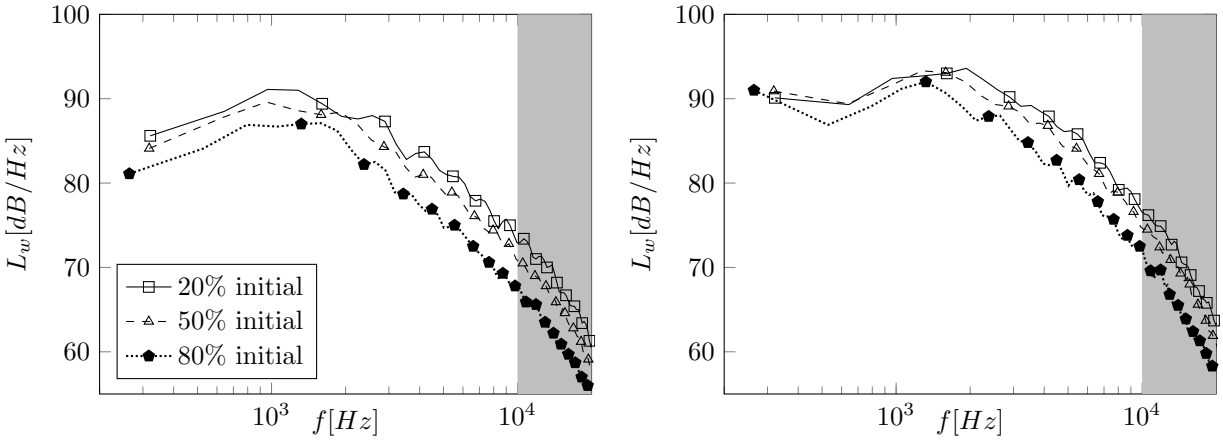

(a) upstream (b) downstream

Figure 12. Initial power spectra at different spanwise positions.

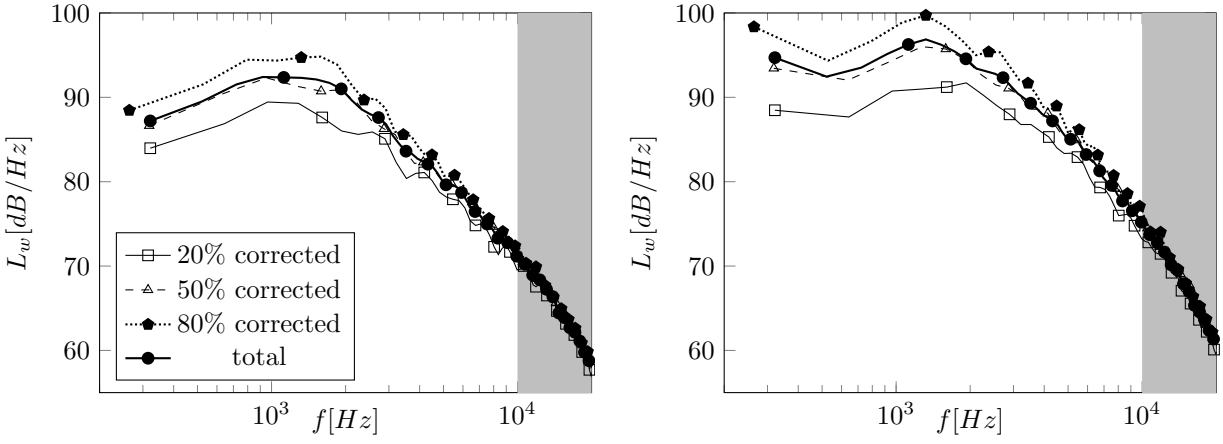

(a) upstream (b) downstream

Figure 13. Corrected power spectra at different spanwise positions as well as total power spectra shown.

To get a more complete description of the sound power level spectra for the entire fan, the acoustic intensity of the three simulations was averaged and used to compute the sound power according to Eq. 6:

$$\overline{I_i} = \frac{1}{3}\sum_{n=1}^{3} I_{i,n}. \tag{13}$$

The total sound power level spectra are shown in Fig. 13. While these total sound power level spectra are still only an approximation of the sound power of the entire duct, a more reliable result can be expected using three spanwise positions instead of only one position. The total sound power spectra are almost identical to those at a stator height of 50%. In fact, the total sound power differs by about 0.5 dB. This confirms that previous 2D CAA computations, that were only performed at the stator midspan, should result in an acceptable approximation for the entire duct if corrections are considered.

Table 4. Sound power levels up- and downstream of stator row at spanwise positions

stator height [%]	final PWL_{up} [dB]	initial PWL_{up} [dB]	final PWL_{down} [dB]	initial PWL_{down} [dB]
20	122.5	124.7	125.9	128.2
50	125.2	123.1	129.2	127.3
80	127.8	120.5	132.2	125.2
Total	**125.7**		**129.8**	

B. Influence of cyclostationarity

In this section, the authors investigated the influence of cyclostationarity in more detail. All studies in this section were performed at 50% of the stator height and no corrections were considered. Firstly, the periodic simulation was compared to two steady simulations, which relied on different averaging techniques for determining the turbulent length scale. The objective was to examine if a steady simulation can reproduce the results of a cyclostationary simulation. Secondly, the periodic approach considers both ingestion noise - resulting from the interaction of the background turbulence with the stator LE's - and RSI - resulting from the interaction of the wake turbulence with the stator LE's. As it is difficult to pinpoint the contribution of these two noise generation mechanisms with a cyclostationary approach, two further simulations were performed to study wake and background turbulence separately.

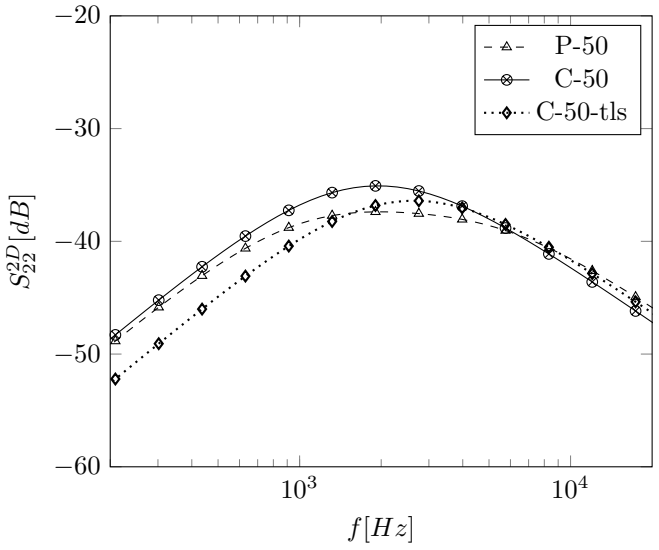

Figure 14. Analytical, 2D upwash velocity frequency spectra shown for simulations P-50, C-50, and C-50-tls.

1. Comparison of periodic and steady simulations

To investigate if the results of a cyclostationary simulation can be reproduced by a simpler simulation relying on circumferentially averaged turbulence statistics and mean flow, two additional simulations were performed: C-50 and C-50-tls (see Table 2). For the C-50 computation, the TLS was computed using the circumferentially averaged TKE, turbulent dissipation rate, and flow velocity as described in Section 3. The

TLS determined by this method was $\Lambda = 0.00958$ m and the averaged TLS, TKE, and mean flow were then prescribed to the CAA and fRPM domains. The C-50-tls also used circumferentially averaged values for the mean flow and the TKE but the TLS was determined using the spectral averaging technique fitted to a von Kármán spectrum (see Section 3). The prescribed TLS using this technique was $\Lambda = 0.00707$ m.

Wohlbrandt et al.[17] have shown that the TLS is the determining factor for cyclostationary simulations and that a constant simulation can exactly reproduce the results of the periodic simulation if a spectrally averaged TLS is prescribed. However, they postulated that this technique only works for cases where the shape of the circumferentially averaged velocity frequency spectrum has the shape of a von Kármán spectrum.

For the ASPIRE configuration at approach conditions, the analytical, 2D upwash velocity frequency spectra are shown for simulations P-50, C-50, and C-50-tls in Fig. 14. This image already shows that an exact fit of the cyclostationary spectrum could not be accomplished as the shape of the P-50 spectrum does not correspond to a von Kármán spectrum. In fact, the velocity spectrum of the P-50 has a much flatter peak region than the spectra of the C-50 and C-50-tls.

It is therefore reasonable that the resulting sound power level spectra of these three simulations did not match (see Fig. 15). The spectral shape of the P-50 simulation differs from the other two simulations. The synthesized, cyclostationary turbulence cannot be described by a von Kármán spectrum. However, it should be noted that the overall sound power of C-50-tls nearly matches the sound power of P-50. Therefore, it is still an improvement compared to the C-50 simulation. This is also confirmed by the total power levels, where the values of the P-50 and C-50-tls simulations are nearly equal (see Table 5).

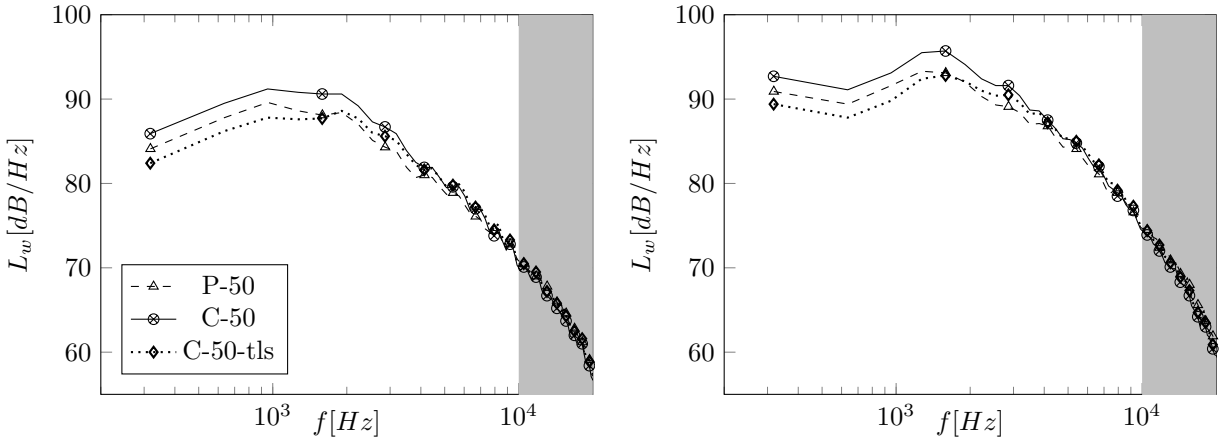

(a) upstream

(b) downstream

Figure 15. Power spectra shown for simulations P-50, C-50, and C-50-tls.

Table 5. Sound power levels for fully periodic and constant simulations at 50% of the stator height.

identifier	PWL_{up} [dB]	P_{up} [W]	PWL_{down} [dB]	P_{down} [W]
P-50	123.1	2.08	127.3	5.51
C-50	125.0	3.18	129.2	8.41
C-50-tls	123.0	2.06	127.4	5.58

It can be concluded that a constant simulation cannot reproduce the results of a cyclostationary simulation at 50% of the stator height. When considering the shapes of the analytical upwash velocity frequency spectra shown in Fig. 8, one can assume that the same is true at the other spanwise positions. All of the velocity spectra have flatter peaks than a von Kármán spectrum. Therefore, considering the cyclostationarity at all spanwise positions was the right approach for predicting the fan broadband noise of the ASPIRE configuration at approach conditions.

2. Contribution of wake and background turbulence to the overall fan broadband noise

The averaged upwash velocity frequency spectrum of the P-50 simulation results from a superposition and averaging of all locally realized spectra spanning a rotor passage. It thus contains spectra that belong to the background turbulence and spectra that belong to the wake turbulence. The simulation therefore inherently contains both ingestion and RSI noise. In this section, the influence of these two noise generation mechanisms on the overall fan broadband noise is studied by performing two additional simulations, which consider wake and background turbulence separately.

To determine an upwash velocity spectrum characterizing wake turbulence, all spectra within the wake were summed up and averaged. The same procedure was applied to determine an upwash velocity spectrum, which describes the background turbulence. The resulting spectra along with the spectrum of the cyclostationary P-50 simulation are shown in Figure 16. The P-50 spectrum is a combination of the C-wake and C-background spectra. Therefore compared to a typical von Kármán spectrum, the P-50 spectrum has a much flatter peak. The C-background spectrum has its peak frequency close to 1.5 kHz, while the C-wake spectrum peaks at a frequency of about 4.5 kHz. The turbulence in the wake causes an increase in amplitude of the averaged velocity frequency spectrum at higher frequencies. The averaged upwash velocity frequency spectrum S_{22}^P can be described in terms of its background S_{22}^b and wake S_{22}^w components as follows:

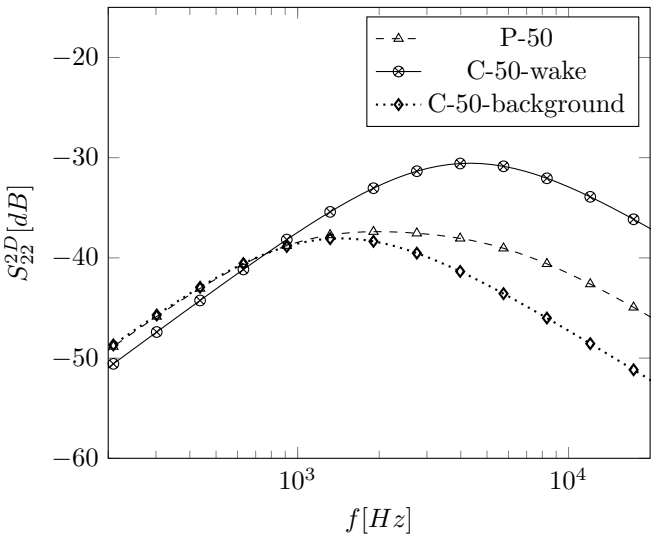

Figure 16. Analytical, 2D upwash velocity frequency spectra shown for simulations P-50, C-50-wake, and C-50-background.

$$S_{22}^P = \widetilde{\theta_w} S_{22}^w + \left(1 - \widetilde{\theta_w}\right) S_{22}^b, \tag{14}$$

where the non-dimensional wake width $\widetilde{\theta_w}$ can be expressed as a function of the wake width θ_w in terms of a circumferential angle and of the number of rotor blades B: $\widetilde{\theta_w} = \frac{\theta_w}{\frac{2\pi}{B}}$. It appears that the background and wake turbulence spectra have a von Kármán shape. Thus, the respective TLS and TKE can be determined by fitting the spectra.

The determined turbulence statistics are prescribed as inputs for simulations C-50-wake and C-50-background. The results of the acoustic simulations are depicted in Figure 17. The behavior of the power level spectra closely resembles the behavior of the upwash velocity frequency spectra. The power level spectra of the C-50-wake simulation is higher in amplitude and its peak frequency is at a higher frequency compared to the power level spectra of the C-50-background simulation. The cyclostationary power level spectra can be expressed in terms of the contributions due to wake and background turbulence:

$$PWL^P = 10 \log \frac{\widetilde{\theta_w} P_w + \left(1 - \widetilde{\theta_w}\right) P_b}{P_{ref}}. \tag{15}$$

The overall sound power can be determined analogously. The overall sound power was used to quantify the contribution of RSI noise, which is caused by the wake turbulence, and the contribution of ingestion noise, which is caused by the background turbulence (see Table 6). The sum of both components is nearly equal to the P-50 simulation as listed in Table 15. In fact, the difference in the sound power level is less than 0.20 dB both up- and downstream of the stator, which shows that Equation 17 is valid for determining the sound power of a cyclostationary simulation. The evaluation of the overall sound powers shows that the fan broadband noise is about 70% ingestion noise and 30% RSI noise. The assumption that the RSI noise is the dominant source in fans is therefore not valid for the investigated case. In fact, the influence of ingestion noise is more critical for the overall fan broadband noise. Thus, both wake and background turbulence

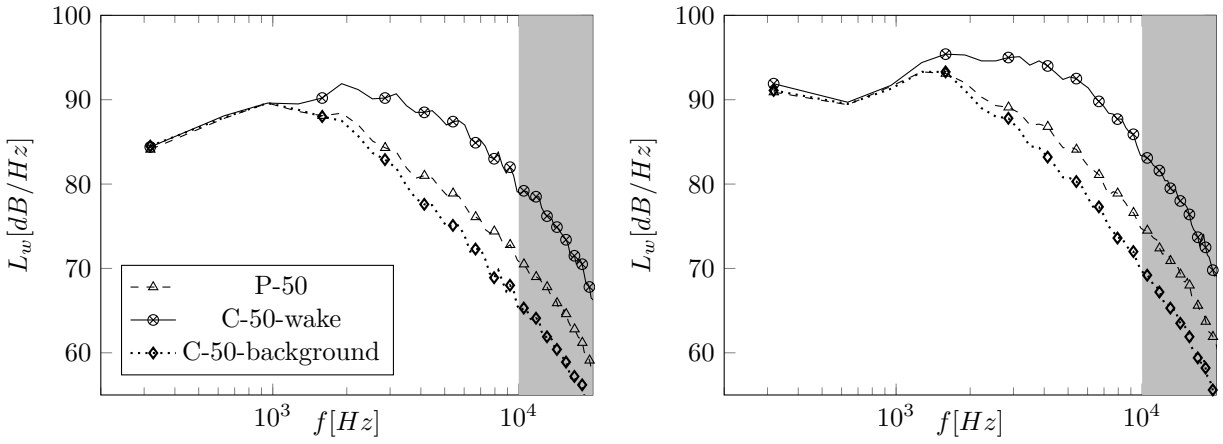

(a) upstream

(b) downstream

Figure 17. Power spectra shown for simulations P-50, C-50-wake, and C-50-background.

have to be considered for the studied fan, which supports the choice of including cyclostationarity in the simulations discussed in Section A.

Table 6. Contribution of wake and background turbulence to the overall fan broadband noise.

identifier	P_{up} [W]	P_{up} [%]	P_{down} [W]	P_{down} [%]
C-50-wake	0.64	29.6	1.79	31.3
C-50-background	1.52	70.4	3.92	68.7
total	**2.16**		**5.71**	

It should be noted that the level of background turbulence - and therefore ingestion noise - depends on the chosen turbulence characteristics at the engine inlet and on the distance from the rotor trailing edge. In this case, the inflow turbulence statistics were chosen to be representative of testbed conditions. If a lower turbulence intensity and a smaller length scale were prescribed, the relevance of ingestion noise would decrease. In addition, the distance from the rotor trailing edge has an influence. If the background turbulence level is not negligibly small, its relative contribution to the overall fan broadband noise increases with an increasing distance from the rotor trailing edge as the wake turbulence fades.

C. Influence of non-linearities

In this work, the authors assumed that non-linearities are negligible and used the linearized Euler equations for the investigations. To check the validity of this hypothesis, an additional simulation (P-50-PENNE) using non-linearized Euler equations was performed. It could be demonstrated that the non-linear terms have no effects on the emitted sound power (see Fig. 18). This proves that the consideration of non-linearities was indeed unnecessary for the investigated configuration.

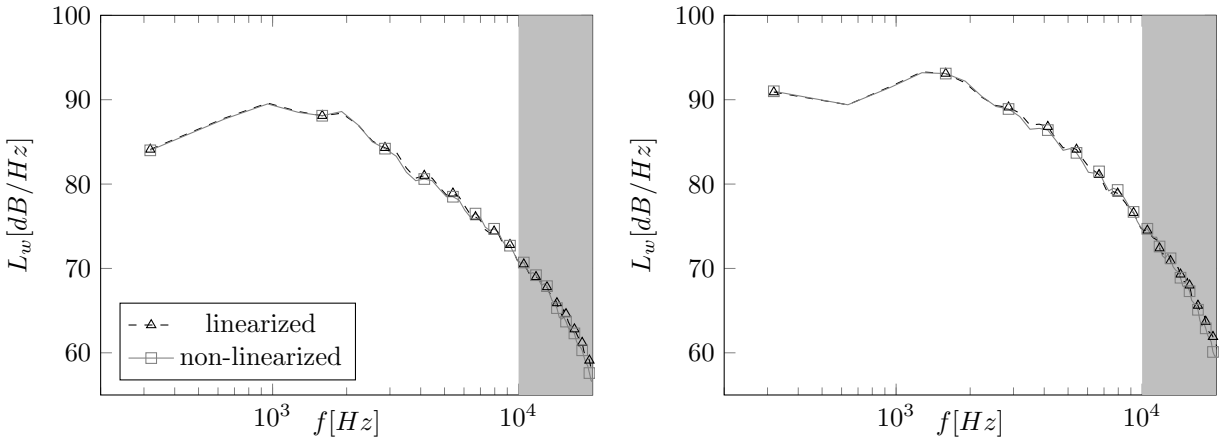

(a) upstream

(b) downstream

Figure 18. Comparison of power spectra shown for CAA simulations with and without non-linear terms.

V. Conclusion

The fRPM-fan method was developed to further the understanding of the broadband RSI noise generation mechanism in a fan stage by enabling the realization of cyclostationarity. The fRPM-fan method combines three distinct methods: A URANS simulation is needed to provide turbulence statistics and a mean flow. The fRPM method synthesizes a turbulence that matches the locally given turbulence statistics in a given mean flow. The turbulent fluctuations are then coupled into the CAA domain. The CAA simulation convects the synthesized turbulence and generates sound. This method cannot only be used in combination with cyclostationarity; simulations relying on circumferentially averaged turbulence statistics and mean flow can also be realized.

In this paper, the 2D fRPM-fan method was applied to study the fan broadband noise in a full-scale, modern fan stage for the first time. In addition, the method was applied at three different spanwise positions and a methodology was introduced to correct for 3D flow effects and for changes in the wake structure between the patch and stator LE position. For the first time, the method was also used in combination with non-linearized Euler equations for a fan application.

The studied test matrix included three simulations at three different spanwise positions. Cyclostationarity was considered and the linearized Euler equations were applied. The other five simulations were performed to confirm the validity of the chosen approach. The key findings of the investigation of fan broadband noise of the ASPIRE fan stage at approach conditions are summarized below:

- The consideration of three spanwise positions and the introduction of a correction technique resulted in a more complete description of the fan broadband noise. As can be expected, the fan broadband noise increased at larger duct radii. The weighting of corrected results at different spanwise position resulted in an increase of about 3 dB in the total sound power up- and downstream of the stator in comparison to uncorrected results obtained at stator midspan. However, when the corrections were taken into account for the 50% stator height position, its sound power deviated by about 0.5 dB from the weighted sound power. Therefore, a midspan position seems to be reasonable.

- The consideration of cyclostationarity was essential for this case as spectrally averaged velocity frequency spectra were not shaped like von Kármán turbulence spectra. Hence, the sound power spectra of a cyclostationary simulation could only be approximated but not reproduced by a constant simulation. It was also shown that both ingestion noise - resulting from the background turbulence - and RSI noise - resulting from the wake turbulence contribute to the overall fan broadband noise. Both are inherently included in a cyclostationary simulation.

- The influence of non-linearities on the fan broadband noise was negligible. No discernible difference can be seen in the sound power level spectra up- and downstream of the fan stage.

One advantage of the fRPM-fan method is that it can be used to investigate different influences on the fan broadband noise individually. This has the potential to further the understanding of the noise generation mechanism and therefore aid in the development and optimization of analytical prediction tools. In the future, this method will be expanded to gain even more insights: The consideration of three spanwise positions yields a more complete description of the noise than relying on only one spanwise position. However, to get a truly complete picture of the noise, an expansion to three-dimensional space is necessary. Instead of correcting for 3D flow effects, these could be considered directly. In addition, an expansion of the fRPM-fan method to anisotropy is envisioned. The method already realizes inhomogeneous turbulence directly and anisotropic turbulence indirectly as the turbulent structures move through high mean flow gradients. However, the turbulence synthesis itself still relies on isotropic turbulence.

Appendix

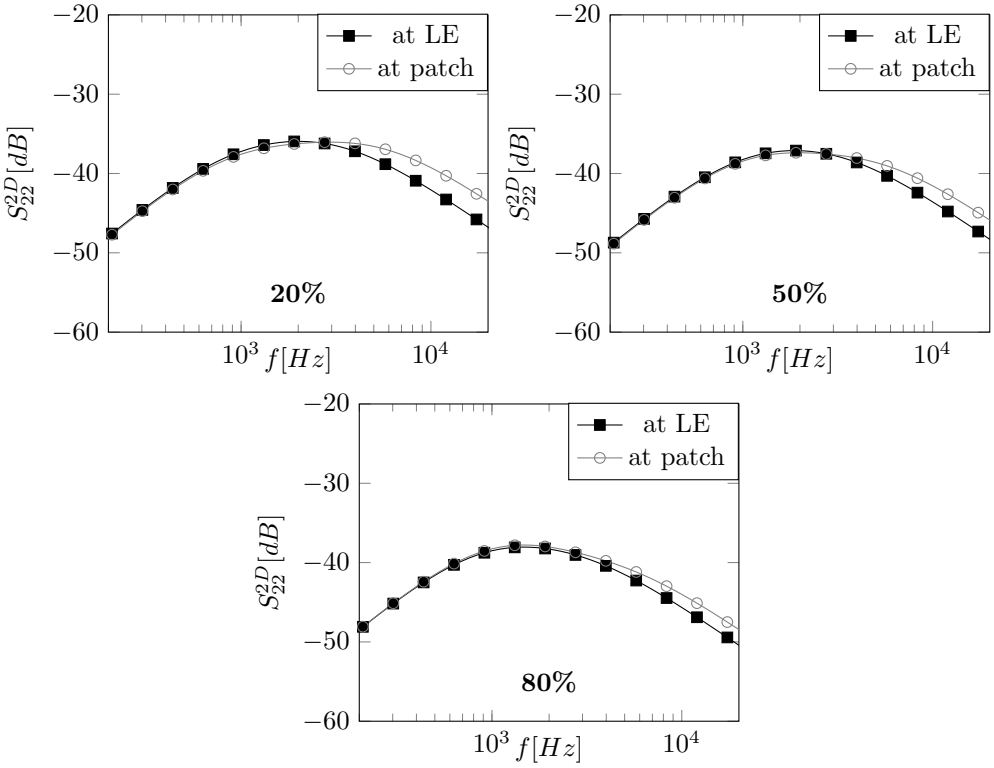

Figure 19. Upwash velocity frequency spectra at leading edge and patch for the determination of the correction curves for changes in the wake.

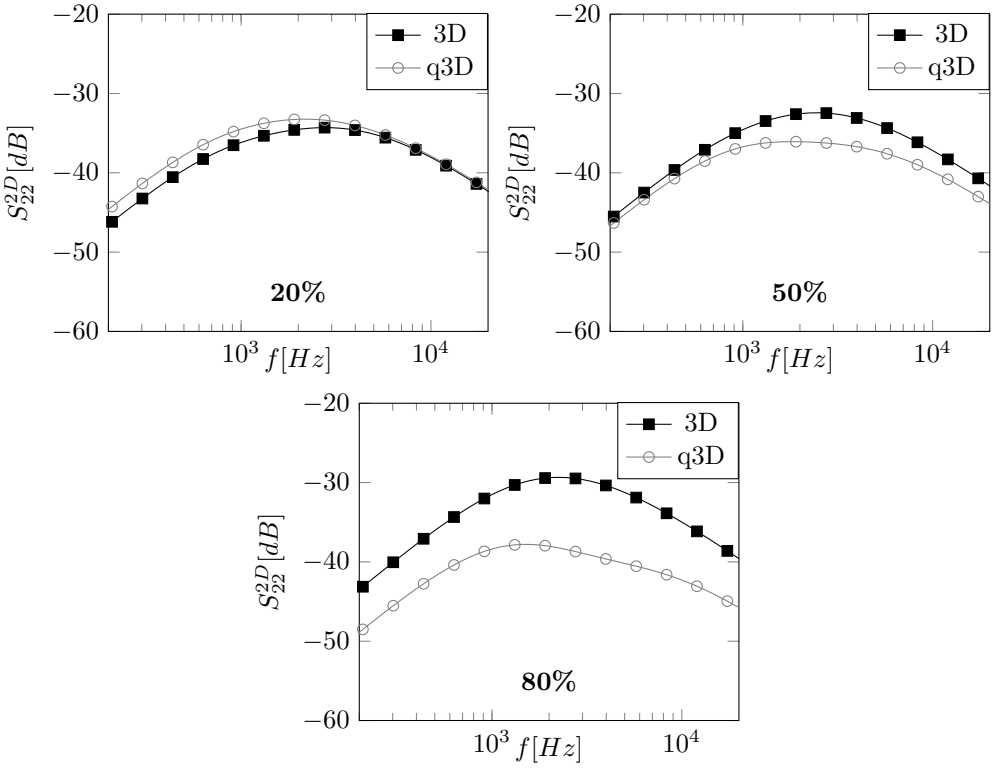

Figure 20. Upwash velocity frequency spectra in 3D and q3D domains for the determination of the correction curves for 3D effects.

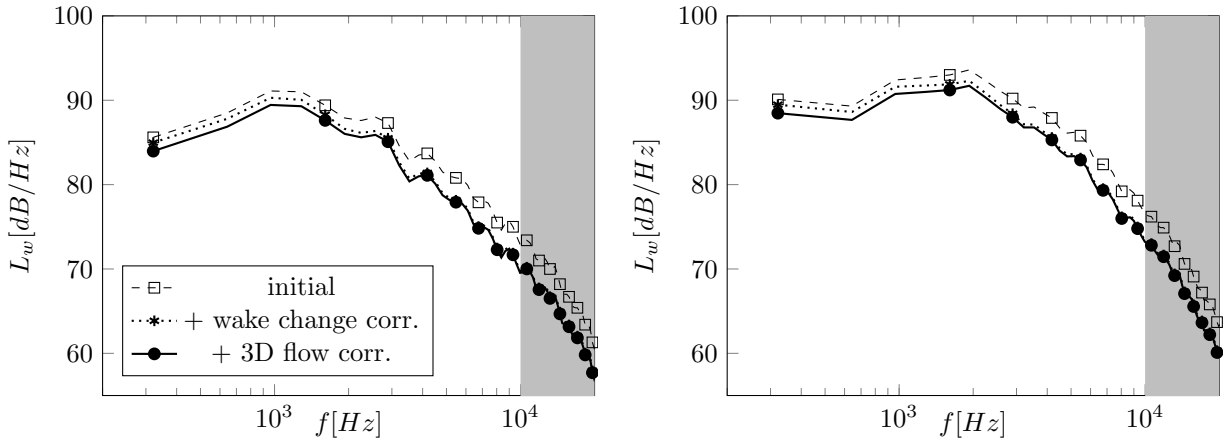

(a) upstream

(b) downstream

Figure 21. Power spectra corrections at 20% of the stator height.

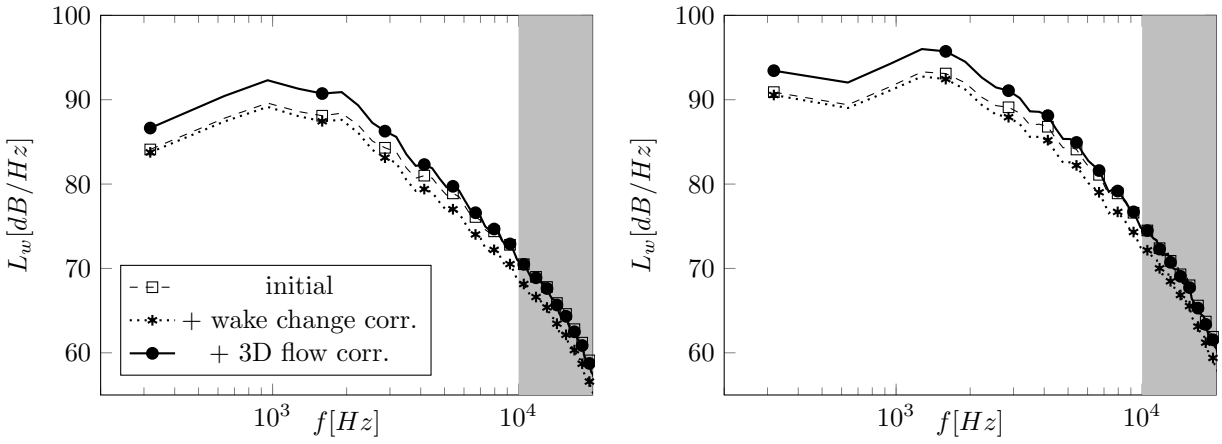

(a) upstream (b) downstream

Figure 22. Power spectra corrections at 50% of the stator height.

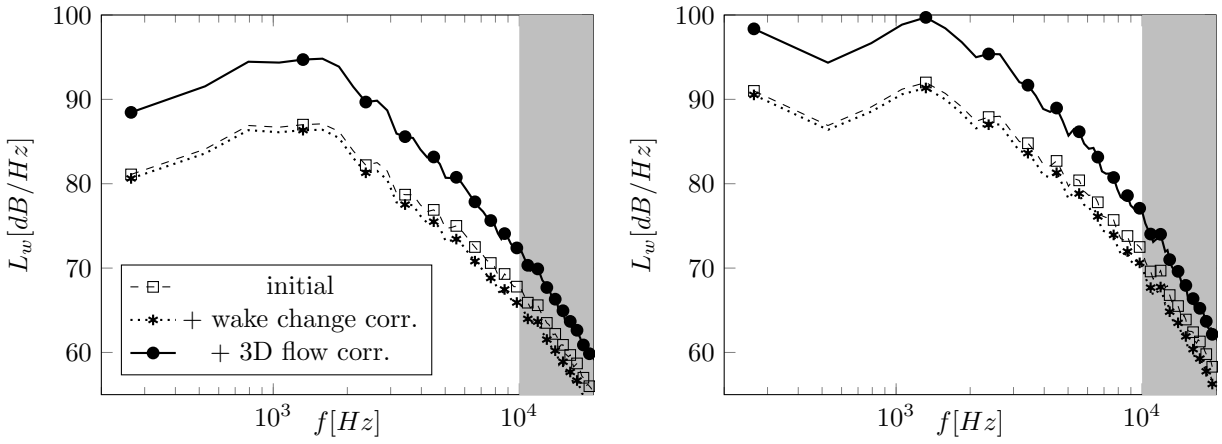

(a) upstream (b) downstream

Figure 23. Power spectra corrections at 80% of the stator height.

Acknowledgments

This project has received funding from the Clean Sky 2 Joint Undertaking under the European Union's Horizon 2020 research and innovation program under grant agreement No 681856 - ASPIRE.

In addition, the authors would like to thank Roland Ewert, Jürgen Dierke, and Nils Reiche (DLR) for their continued support and advice.

References

[1]Kraichnan, R. H., "Diffusion by a random velocity field," *Physics of Fluids (1958-1988)*, Vol. 13, No. 1, 1970, pp. 22–31.

[2]Bechara, W., Bailly, C., Lafon, P., and Candel, S. M., "Stochastic approach to noise modeling for free turbulent flows," *AIAA Journal*, Vol. 32, No. 3, 1994, pp. 455–463.

[3]Billson, M., Eriksson, L.-E., and Davidson, L., "Jet noise prediction using stochastic turbulence modeling," *9th AIAA/CEAS Aeroacoustics Conference*, Hilton Head, South Carolina, 2003.

[4]Clair, V., Polacsek, C., Le Garrec, T., and Reboul, G., "CAA methodology to simulate turbulence-airfoil noise," *18th AIAA/CEAS Aeroacoustics Conference*, Colorado Springs, Colorado, 2012.

[5]Amiet, R. K., "Acoustic radiation from an airfoil in a turbulent stream," *Journal of Sound and Vibration*, Vol. 41, No. 4, Aug. 1975, pp. 407–420.

[6]Gill, J., Zhang, X., Joseph, P., and Nodé-Langlois, T., "Reduced dimension modeling of leading edge turbulent interaction noise," *20th AIAA/CEAS Aeroacoustics Conference*, 2014.

[7]Polacsek, C., Clair, V., Le Garrec, T., Reboul, G., and Jacob, M. C., "Numerical predictions of turbulence/cascade-interaction noise using computational aeroacoustics with a stochastic model," *AIAA Journal*, Vol. 53, No. 12, 2015, pp. 3551–3566.

[8]Namba, M. and Schulten, J., "Category 4-fan stator with harmonic excitation by rotor wake," *Third Computational Aeroacoustics (CAA) Workshop on Benchmark Problems (ed. JC Hardin, D. Huff & CK Tam)*, Citeseer, 2000, pp. 73–86.

[9]Reboul, G., Cader, A., Polacsek, C., Le Garrec, T., Barrier, R., and Nasr, N. B., "CAA Prediction of Rotor-Stator Interaction Using Synthetic Turbulence: Application to a Low-Noise Serrated OGV," *23rd AIAA/CEAS Aeroacoustics Conference*, 2017.

[10]Jarrin, N., Benhamadouche, S., Laurence, D., and Prosser, R., "A synthetic-eddy-method for generating inflow conditions for large-eddy simulations," *International Journal of Heat and Fluid Flow*, Vol. 27, No. 4, Aug. 2006, pp. 585–593.

[11]Sescu, A. and Hixon, R., "Toward low-noise synthetic turbulent inflow conditions for aeroacoustic calculations," *International Journal for Numerical Methods in Fluids*, Vol. 73, No. 12, 2013, pp. 1001–1010.

[12]Kim, J. W. and Haeri, S., "An advanced synthetic eddy method for the computation of aerofoil-turbulence interaction noise," *Journal of Computational Physics*, Vol. 287, 2015, pp. 1–17.

[13]Gea-Aguilera, F., Zhang, X., Chen, X., Gill, J. R., and Nodé-Langlois, T., "Synthetic turbulence methods for leading edge noise predictions," *21st AIAA/CEAS Aeroacoustics Conference, Dallas, USA*, 2015.

[14]Gea Aguilera, F., Gill, J., Zhang, X., Chen, X., and Nodé-Langlois, T., "Leading Edge Noise Predictions Using Anisotropic Synthetic Turbulence," *22nd AIAA/CEAS Aeroacoustics Conference*, 2016, p. 2840.

[15]Podboy, G. G., Krupar, M. J., Helland, S. M., and Hughes, C. E., "AIAA2002-1033 Steady and Unsteady Flow Field Measurements Within a NASA 22 Inch Fan Model," 2001.

[16]Gea-Aguilera, F., Gill, J., Angland, D., and Zhang, X., "Wavy Leading Edge Airfoils Interacting with Anisotropic Turbulence," *23rd AIAA/CEAS Aeroacoustics Conference*, 2017.

[17]Wohlbrandt, A., Kissner, C., and Guérin, S., "Impact of cyclostationarity on fan broadband noise prediction," *Journal of Sound and Vibration*, Vol. 420, April 2018, pp. 142–164.

[18]Ewert, R., Dierke, J., Siebert, J., Neifeld, A., Appel, C., Siefert, M., and Kornow, O., "CAA broadband noise prediction for aeroacoustic design," *Journal of Sound and Vibration*, Vol. 330, No. 17, 2011, pp. 4139–4160.

[19]Ganz, U. W., Joppa, P. D., Patten, T. J., and Scharpf, D. F., "Boeing 18-inch fan rig broadband noise test," 1998.

[20]Jurdic, V., Joseph, P., and Antoni, J., "Investigation of rotor wake turbulence through cyclostationary spectral analysis," *AIAA Journal*, Vol. 47, No. 9, 2009, pp. 2022–2030.

[21]Becker, K., Heitkamp, K., and Kügeler, E., "Recent Progress in a Hybrid Grid CFD Solver for Turbomachinery Flows," *Proc. V European Conference on Computational Fluid Dynamics ECCOMAS CFD 2010*, Lisbon, Portugal, 2010.

[22]Cécora, R.-D., Radespiel, R., Eisfeld, B., and Probst, A., "Differential Reynolds-stress modeling for aeronautics," *AIAA Journal*, 2015.

[23]Wohlbrandt, A., Hu, N., Guérin, S., and Ewert, R., "Generalised turbulence spectra for broadband noise predictions with the Random Particle Mesh method," *Computers and Fluids*, Vol. 132, 2016, pp. 46–50.

[24]Siefert, M. and Ewert, R., "Sweeping Sound Generation in Jets Realized with a Random Particle-Mesh Method," *15th AIAA/CEAS Aeroacoustics Conference*, 2009.

[25]Delfs, J. W., Bauer, M., Ewert, R., Grogger, H., Lummer, M., and Lauke, T., "Numerical Simulation of Aerodynamic Noise with DLR's aeroacoustic code PIANO," Tech. rep., German Aerospace Center (DLR), Braunschweig, Jan. 2008.

[26]Hu, F. Q., Hussaini, M. Y., and Manthey, J. L., "Low-dissipation and low-dispersion Runge - Kutta schemes for computational acoustics," *Journal of Computational Physics*, Vol. 124, No. 1, 1996, pp. 177–191.

[27]Tam, C. K. and Webb, J. C., "Dispersion-relation-preserving finite difference schemes for computational acoustics," *Journal of Computational Physics*, Vol. 107, No. 2, 1993, pp. 262–281.

[28]Long, L. N., "A nonconservative nonlinear flowfield splitting method for 3-D unsteady fluid dynamics," *AIAA paper*, Vol. 1998, 2000.

[29]Ewert, R., Dierke, J., Neifeld, A., and Moghadam, S. A., "Linear-and Non-Linear Perturbation Equations with Relaxation Source Terms for Forced Eddy Simulation of Aeroacoustic Sound Generation," *AIAA Paper*, Vol. 3053, 2014.

[30]Grace, S., Maunus, J., and Sondak, D. L., "Effect of CFD Wake Prediction in a Hybrid Simulation of Fan Broadband Interaction Noise," No. AIAA 2011-2875 in 17th AIAA/CEAS Aeroacoustics Conference, Oregon, Portland, USA, 2011.

[31]Donzis, D. A., Sreenivasan, K. R., and Yeung, P., "Scalar dissipation rate and dissipative anomaly in isotropic turbulence," *Journal of Fluid Mechanics*, Vol. 532, 2005, pp. 199–216.

[32]Blandeau, V. P., Joseph, P. F., Jenkins, G., and Powles, C. J., "Comparison of sound power radiation from isolated airfoils and cascades in a turbulent flow," *The Journal of the Acoustical Society of America*, Vol. 129, No. 6, 2011, pp. 3521–3530.

[33]De Roeck, W., Desmet, W., Baelmans, M., and Sas, P., "An overview of high-order finite difference schemes for computational aeroacoustics," *Proceedings of the International Conference on Noise and Vibration Engineering*, Citeseer, 2004, pp. 353–368.